Impact of SiC Devices on Hybrid Electric and Plug-In Hybrid Electric Vehicles

Hui Zhang, *Member, IEEE*, Leon M. Tolbert, *Senior Member, IEEE*, and Burak Ozpineci, *Senior Member, IEEE*

***Abstract*—The application of silicon carbide (SiC) devices as battery interface, motor controller, etc., in a hybrid electric vehicle (HEV) will be beneficial due to their high-temperature capability, high-power density, and high efficiency. Moreover, the light weight and small volume will affect the whole powertrain system in a HEV and, thus, the performance and cost. In this paper, the performance of HEVs is analyzed using the vehicle simulation software Powertrain System Analysis Toolkit (PSAT). Power loss models of a SiC inverter based on the test results of latest SiC devices are incorporated into PSAT powertrain models in order to study the impact of SiC devices on HEVs from a system standpoint and give a direct correlation between the inverter efficiency and weight and the vehicle's fuel economy. Two types of HEVs are considered. One is the 2004 Toyota Prius HEV, and the other is a plug-in HEV (PHEV), whose powertrain architecture is the same as that of the 2004 Toyota Prius HEV. The vehicle-level benefits from the introduction of SiC devices are demonstrated by simulations. Not only the power loss in the motor controller but also those in other components in the vehicle powertrain are reduced. As a result, the system efficiency is improved, and vehicles that incorporate SiC power electronics are predicted to consume less energy and have lower emissions and improved system compactness with a simplified thermal management system. For the PHEV, the benefits are even more distinct; in particular, the size of the battery bank can be reduced for optimum design.**

***Index Terms*—Efficiency, hybrid electric vehicle (HEV), inverter, plug-in HEV (PHEV), Powertrain System Analysis Toolkit (PSAT), silicon carbide (SiC).**

I. Introduction

As THE issues of natural resource depletion and environmental impacts have gained greater visibility, the hybrid electric vehicle (HEV) market has rapidly expanded [1]–[5]. The application of SiC devices (as battery interface, motor controller, etc.) in a HEV has merit because of their high-temperature capability, high-power density, and high efficiency, which has been indicated by some previous works [6]–[8]. However, aside from these inverter-level benefits, the applications of SiC inverters/converters also affect the performance of other components in the powertrain system, and thus their design and cost, due to the inverters/converters' high efficiency, light weight, and small volume. This has not been addressed clearly yet. Therefore, this paper provides a quantitative vehicle-level impact of SiC devices for HEVs in addition to inverter-level illustration by using complete system modeling, which is unlike some system models developed in other works that are solely for inverter simulation [9], [10]. Such complete system modeling is built and implemented in Powertrain System Analysis Toolkit (PSAT).

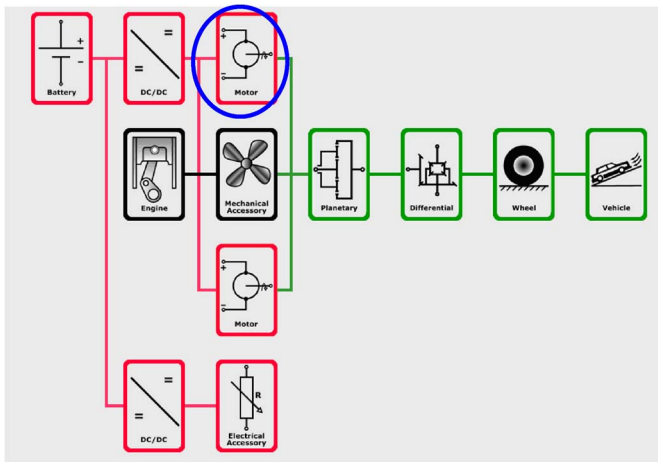

Fig. 1. Powertrain architecture of 2004 Toyota Prius HEV.

PSAT is vehicle simulation software based on MATLAB Simulink developed by Argonne National Laboratory, which can evaluate how different powertrain and vehicle design architectures affect HEVs [11]. In this paper, power loss models of a SiC inverter are incorporated into PSAT models in order to study the impact of SiC devices on HEVs. Two types of HEVs are considered. One is the 2004 Toyota Prius HEV, which has a split powertrain architecture shown in Fig. 1. The other is a plug-in HEV (PHEV), whose powertrain architecture is similar to that of the 2004 Toyota Prius HEV but has a pure electrical operation range. SiC devices are applied to the primary motor marked in Fig. 1 as a three-phase dc/ac inverter to take the place of the conventional silicon (Si) inverter. The development of device models, power loss models, thermal models, system models, and simulations on such systems will be discussed in detail in this paper. Both inverter- and vehicle-level benefits

Manuscript received October 9, 2009; revised March 1, 2010 and June 14, 2010; accepted July 24, 2010. Date of publication December 30, 2010; date of current version March 18, 2011. Paper 2009-PEDCC-328.R2, presented at the 2008 Industry Applications Society Annual Meeting, Edmonton, AB, Canada, October 5–9, and approved for publication in the IEEE TRANSACTIONS ON INDUSTRY APPLICATIONS by the Power Electronics Devices and Components Committee of the IEEE Industry Applications Society.

H. Zhang is with the Electrical Engineering Department, Tuskegee University, Tuskegee, AL 36088 USA (e-mail: hzhang18@ieee.org).

L. M. Tolbert is with the Department of Electrical Engineering and Computer Science, The University of Tennessee, Knoxville, TN 37996-2100 USA, and also with the Power Electronics and Electric Machinery Research Center, Oak Ridge National Laboratory, Knoxville, TN 37932 USA (e-mail: tolbert@utk.edu).

B. Ozpineci is with the Power Electronics and Electric Power Systems Research Center, Oak Ridge National Laboratory, Knoxville, TN 37932 USA (e-mail: ozpinecib@ornl.gov).

Color versions of one or more of the figures in this paper are available online at http://ieeexplore.ieee.org.

Digital Object Identifier 10.1109/TIA.2010.2102734

from the introduction of the SiC devices will be demonstrated. Compared to our previous work [12], discussions in this paper are based on the measured qualities of SiC devices instead of predicted characteristics using device physics models.

II. SiC Device Characterization and Modeling

Since the manufacturers provide datasheets for commercially available SiC Schottky diodes, this section focuses on SiC JFETs. The latest SiC JFETs have been obtained from SiCED and tested for both static and dynamic characteristics. Based on these experimental results, numerical models are developed for use in the simulations. The detailed information will be given in the following paragraphs.

A. Static Tests

A curve tracer Tektronix 371B was used to obtain the forward and transfer characteristics. The SiC JFETs were put into an environmental chamber to raise the ambient temperature up to 175 °C in 25 °C increments. The static characteristics of the SiC JFETs are shown in Fig. 2. As shown in the figure, the ON-state resistance of the SiC JFETs increases with temperature from 25 °C to 175 °C, and the transfer characteristics of the devices are nearly constant in this temperature range.

Since the manufacturer did not specify the current rating for these devices, the characteristics of the SiC JFETs are compared to some similar SiC devices with the specified current rating. One of these devices is a SiC JFET (1200 V/5 A) from SemiSouth, and the other is a SiC MOSFET (1200 V/10 A) from CREE. The ON-state resistances and switching losses are plotted in Fig. 3. As shown in Fig. 3, the characteristics of the SiC JFETs are very close to those of the 5-A JFETs from SemiSouth. If two of the SiC JFETs are used in parallel, the characteristics of such a group of SiC JFETs will be close to those of the 10-A SiC MOSFETs from CREE. Thus, it is safe to use these SiC JFETs from SiCED as 5-A devices. Furthermore, the chip size of these SiC JFETs is about 0.1467 cm^2. Correspondingly, the specific heat dissipation values of these devices are about 57.4 W/cm^2 for the switching frequency of 20 kHz at 100 °C and 72.4 W/cm^2 at 175 °C.

In addition, as shown in Fig. 2, the I–V characteristic of the SiC JFETs is nonlinear. When the current exceeds 5 A, the nonlinearity becomes obvious and is more dramatic for higher temperatures. It indicates that the ON-state resistance increases with increasing current when the current is larger than 5 A, and at higher temperatures, the more quickly it increases. More specifically, at 175 °C, the ON-state resistance increases by 30% (324 mΩ at 5 A to 420 mΩ at 12 A) when the current changes from 5 to 12 A. Considering the high-temperature condition in HEVs and the comparison to other similar SiC devices, it is reasonable to use the devices as 5-A devices in these applications. The simulations shown in this paper are based on this assumption. Thus, the quantitative results obtained here demonstrate an efficiency-optimized use of these SiC JFETs as a replacement for Si devices. For practical applications with specific requirements on efficiency, temperature, space, and cost, a set of simulations can be done with different numbers

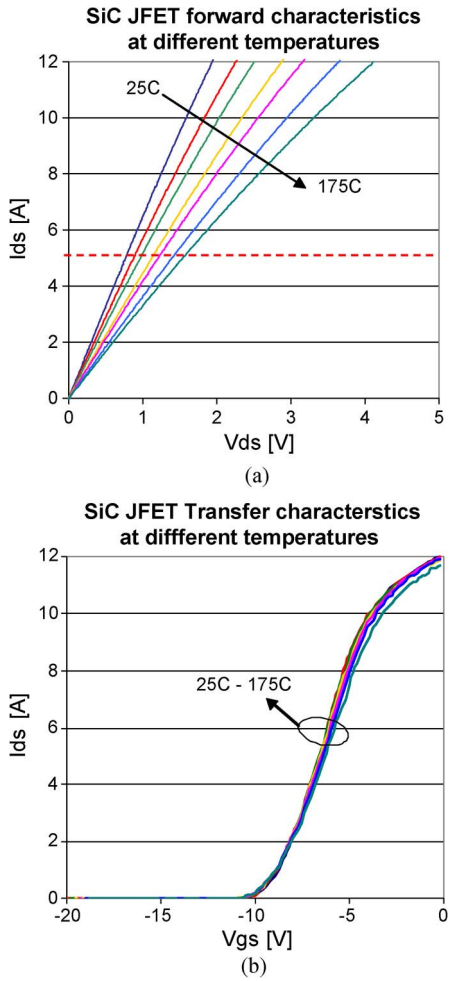

Fig. 2. Static characteristics of the SiC JFET (SiCED). (a) Forward characteristics. (b) Transfer characteristics.

of devices using the method presented in this paper in order to determine the optimized number of devices in parallel and corresponding quantitative results.

With the assumption of 5-A rating, the ON-state resistance of the SiC JFETs is constant with respect to current and is a function of device junction temperature. By letting it be a quadratic function, the ON-state resistance can be represented as

$$R_{J,\mathrm{on}} = 0.0021T^2 + 0.5981T + 141.57\ (\mathrm{m}\Omega) \qquad (1)$$

where the coefficients are obtained by performing curve fitting on test results shown in Fig. 2(a). Similar equations can be established for the ON-state resistance of SiC Schottky diodes based on the manufacturer's data or test results [13].

B. Switching Tests

The test circuit shown in Fig. 4 is used for the switching tests. It has a pure inductive load. The switch is controlled by a double-pulse signal, and the current in it can be changed by varying the duty ratio of the first pulse.

The SiC JFETs from SiCED are normally on devices, which require a negative voltage to turn off. Commercial gate driver

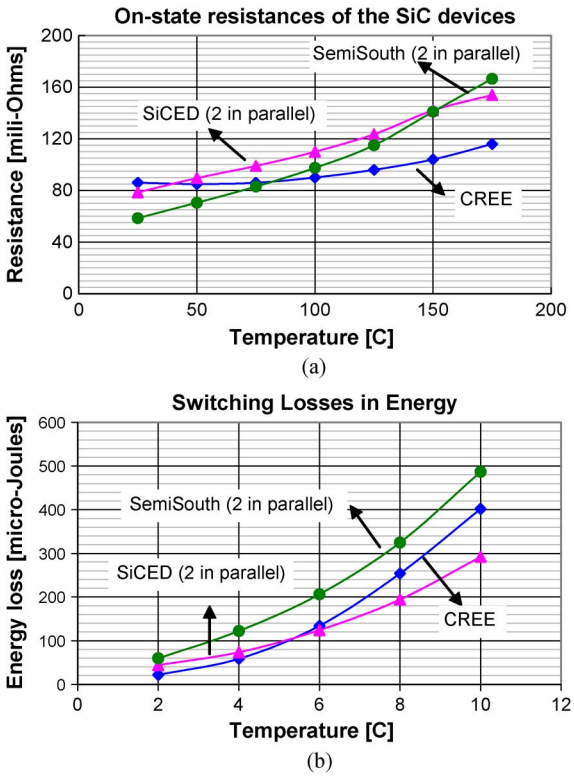

Fig. 3. Characteristics of sample SiC switches. (a) ON-state resistances. (b) Switching losses in energy.

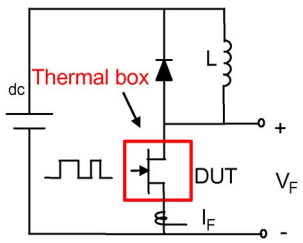

Fig. 4. Switching circuit for double-pulse switch testing.

IC HCNW3120 was used to generate such a signal with a positive voltage of 0 V and a negative voltage of −18 V. The gate signal waveforms when using a gate resistance of 10 Ω are shown in Fig. 5(a). To observe the temperature effect on the switching behavior, the devices are put into a chamber to raise the junction temperature up to 175 °C. The switching waveforms of the devices at the test condition of 200 V, 5 A, and 175 °C are also shown in Fig. 5(b). The switching energy losses at different temperatures and current levels are calculated and plotted in Fig. 6. It indicates that the switching losses increase with increasing current and are nearly constant with increasing temperature. Thus, the switching energy loss can be a polynomial function of current since its change with temperature is negligible, which can be calculated as

$$E_{J,\mathrm{sw}}(i) = 0.9932i^3 - 3.6578i^2 + 22.755i \ (\mathrm{mJ}). \quad (2)$$

Similar to (1), the coefficients in (2) are also obtained by performing curve fitting on test results shown in Fig. 6(b).

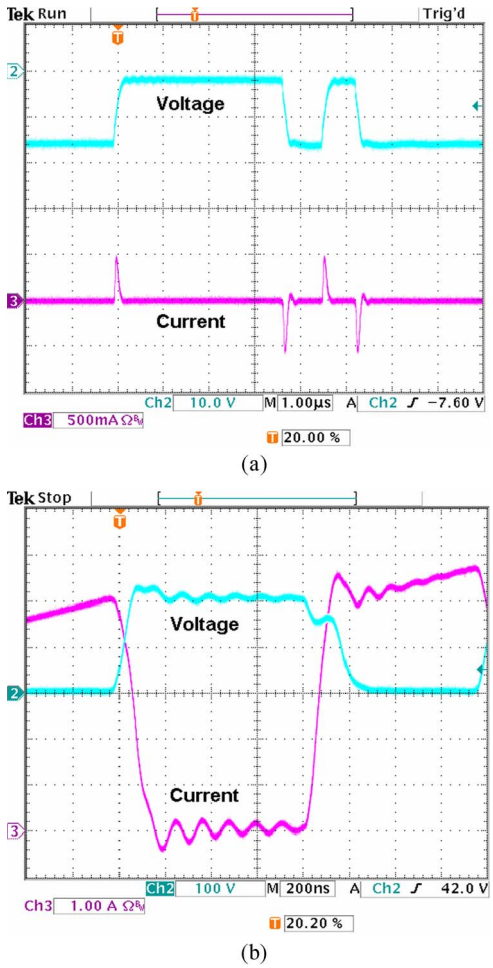

Fig. 5. Switching test waveforms of the SiC JFET (SiCED). (a) Gate signal waveforms. (b) Switching waveforms at 175 °C.

In addition to the dependence of switching losses on current as shown in (2), the switching losses in SiC JFETs are also affected by the applied voltage. This effect can be accounted for by introducing a factor corresponding to the ratio between the applied voltage and the test voltage at which the switching losses are measured [14]; for this case, the test voltage is 200 V. This ratio is reflected in (4) in Section III.

Similarly, the change of switching losses with voltage in SiC Schottky diodes is also accounted for by introducing such a factor (see (6) in Section III). Moreover, this change is the only one which needed to be considered for a SiC Schottky diode operating under different conditions because its switching losses (mainly reverse recovery loss) are more dependent on voltage than current and do not vary with temperature [15].

III. Modeling and Validation

PSAT provides a programming environment based on MATLAB for HEVs, but it does not include a separate inverter model. In order to simulate using different inverter designs, the built-in motor/inverter model is revised, and a new inverter model which has the capability to calculate its power loss and efficiency is created using MATLAB Simulink. Fig. 7(a)

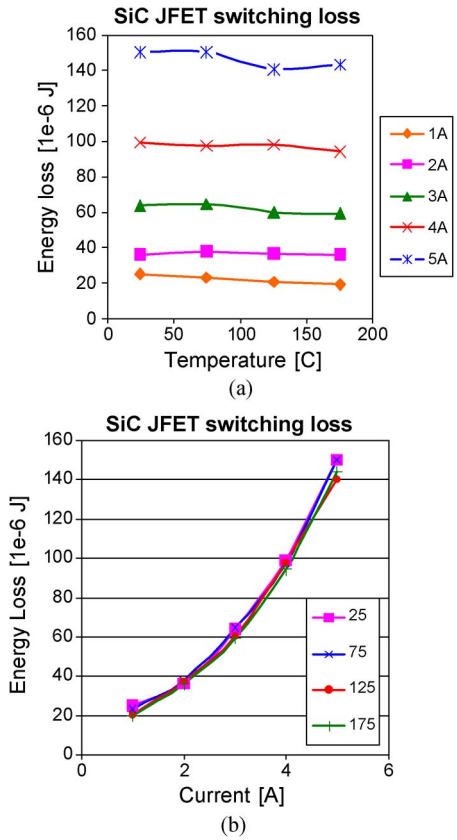

Fig. 6. Switching loss of the SiC JFET at different conditions. (a) Energy loss versus temperature at different current levels. (b) Energy loss versus current at different temperatures.

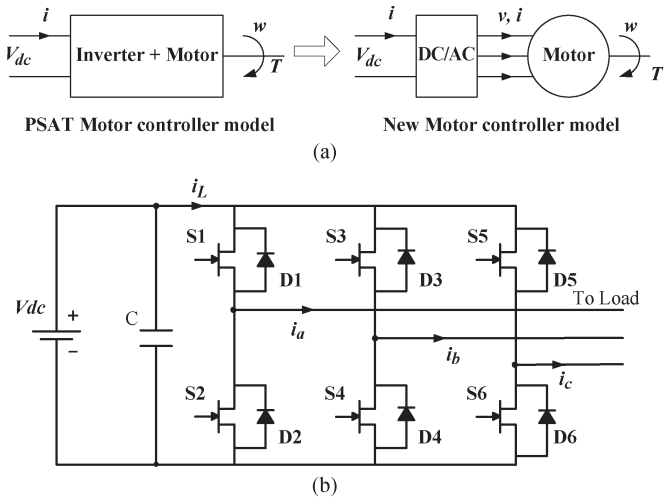

Fig. 7. (a) Comparison of PSAT model and the new model. (b) Topology of a standard three-phase full-bridge converter.

compares the new model to the PSAT model. The layout of the inverter is shown in Fig. 7(b), which is composed of six SiC JFETs and six SiC Schottky diodes.

The devices listed in Table I represent the SiC semiconductor technology whose characteristics and related models have been presented in Section II. By paralleling these devices, an inverter at a power rating required by the vehicle systems is formed

TABLE I
DEVICES USED IN THE CONVERTERS

Item	Voltage rating	Current rating	Part number
SiC JFETs	1200	5A×60	SiCED
SiC Schottky diodes	1200	10A×30	CREE, CSD10120
Si IGBT Module	1200	300A	Powerex, CM300DY-24NF

Note: multiples represent the number of devices in parallel; current ratings are for temperature > 100 °C .

and used in the simulations. However, the practical use of SiC devices in such systems can only be enabled by more advanced technologies which can provide devices with a large enough power rating due to the difficulty of paralleling devices and resultant complexity. Presently, many research efforts have been made to improve the single-device rating [16], [17] and develop high-power modules [18]–[23]. The single SiC diode and double-diffused MOSFET voltage rating is up to 10 kV with a die area exceeding 1.5 and 0.64 cm^2, respectively [16].

The largest SiC power modules reported in the literature are 10 kV/100 A [20] and 1.2 kV/880 A [17]. It is promising that SiC inverters with a comparable rating to present Si IGBT-based inverters can be realized in the near future. Thus, based on the current device quality, this paper tries to provide a prediction of what will be achievable when using SiC devices in the near future under the following two assumptions: (1) Future SiC devices will have the same performance with today's SiC devices, and (2) module packaging technology does not introduce parasitics or issues other than those found in single-device packaging. The first assumption is a conservative one, while the latter one is overly optimistic. Thus, the actual performance will vary some from the predicted performance in future SiC inverters and depends on the continued future device development and packaging technologies for large current-rated modules.

Based on the single-device models discussed in the previous section, an averaging technique [24], [25] is applied to calculate the effective power losses of devices based on a fundamental motor voltage period in an inverter controlled by a sinusoidal pulse width modulation technique. The specific equations for SiC inverters, whose symbols are given in the Appendix, are presented in the following:

$$P_{J,\text{cond}} = I^2 R_{J,\text{on}} \left(\frac{1}{8} \pm \frac{1}{3\pi} M \cos\phi \right) \tag{3}$$

$$P_{J,\text{sw}} = f_s \cdot \left(\frac{V}{V_0} \right)^{\frac{3}{2}} \cdot (0.2108 I^3 - 0.9144 I^2 + 7.2431 I) \times 10^{-6} \tag{4}$$

$$P_{D,\text{cond}} = I^2 \cdot R_{D,\text{on}} \left(\frac{1}{8} \mp \frac{1}{3\pi} M \cos\phi \right) + I \cdot V_D \cdot \left(\frac{1}{2\pi} \mp \frac{M \cos\phi}{8} \right) \tag{5}$$

$$P_{D,\text{sw}} = f_s \frac{V}{4S} \sqrt{\frac{V}{V_0}} \left(\frac{dI}{dt} \right) \left(\frac{S t_{\text{rr}}}{S+1} \right)^2 \tag{6}$$

where the lower sign of the double sign is applied for motor regeneration. Then, the power loss of an inverter is the sum of

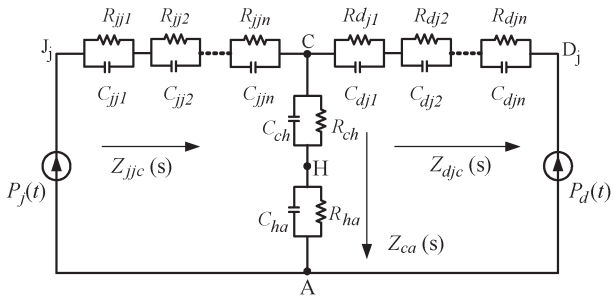

Fig. 8. Thermal equivalent circuit of an inverter.

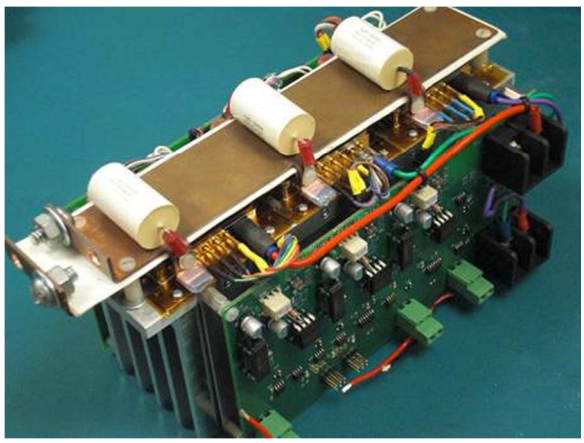

Fig. 9. SiC JFET inverter prototype.

the conduction loss (3) and switching loss (4) of the JFETs and the conduction loss (5) and switching loss (6) of the diodes. Since there are six of the JFETs and diodes in an inverter and they are assumed to be identical, the total power loss of an inverter is

$$P_{\mathrm{Inv,SiC}} = 6 \times (P_{J,\mathrm{cond}} + P_{J,\mathrm{sw}} + P_{D,\mathrm{cond}} + P_{D,\mathrm{sw}}). \quad (7)$$

To count the self-heating of devices in the inverter, the thermal equivalent circuit shown in Fig. 8 is incorporated into the inverter model. Power losses at current temperature are fed to this model to calculate new device junction temperatures for the next computation iteration in order to update power losses based on the new temperature. In this way, the self-heating of the devices is accounted for dynamically. As shown in the figure, the power sources of the circuit are the power losses (P_j and P_d) from switches and diodes (assumed to be on the same heat sink), and the interfaces between the junctions of these devices, heat sink, and thermal grease are modeled as a series of RC pairs [14], [26], [27]. This circuit can be solved using transfer functions in the frequency domain. Parameters used in this model are directly found or extracted from manufacturer data [28].

As a validation of the inverter models presented in this paper, the same model is used to estimate the efficiency of a SiC JFET inverter prototype shown in Fig. 9, which is composed of three phase-leg modules (three SiC JFETs in parallel and one antiparalleled diode) [29]. The efficiency of this inverter obtained from

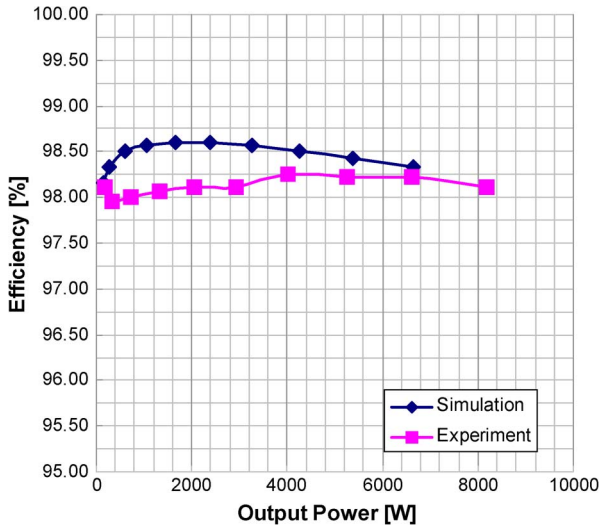

Fig. 10. Efficiency of the SiC JFET inverter.

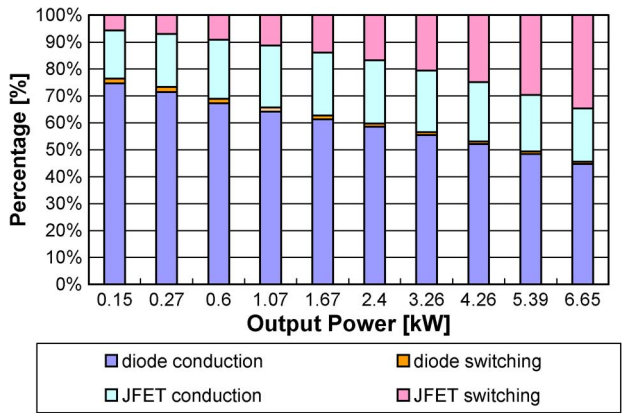

Fig. 11. Percentage of power losses in the SiC inverter at the junction temperature of 100 °C and the switching frequency of 10 kHz.

simulations is compared to that from experiments in Fig. 10 for the following operating condition: an output fundamental frequency of 60 Hz, a modulation index of 0.85, an RL load of 10 Ω and 1.2 mH, and a variable dc side voltage from 75 to 500 V. The maximum error is about 1%. Thus, the model used in this paper should fairly well represent losses for the HEV simulations. Furthermore, the conduction losses are more dominant for both diodes and JFETs compared to switching losses; in particular, the switching losses of diodes are almost negligible.

All increases in current, voltage, and switching frequency will contribute to the increasing switching losses in the JFETs (see Figs. 11 and 12). The behaviors of SiC devices in the simulated motor controller are similar to this.

With the inverter models presented here, the system program for the HEVs can be generated by PSAT, which is shown in Fig. 13. It is composed of a driver, a vehicle controller, a component controller, and powertrain models. Simulations of the HEV and PHEV will be conducted and discussed in Sections IV and V, respectively.

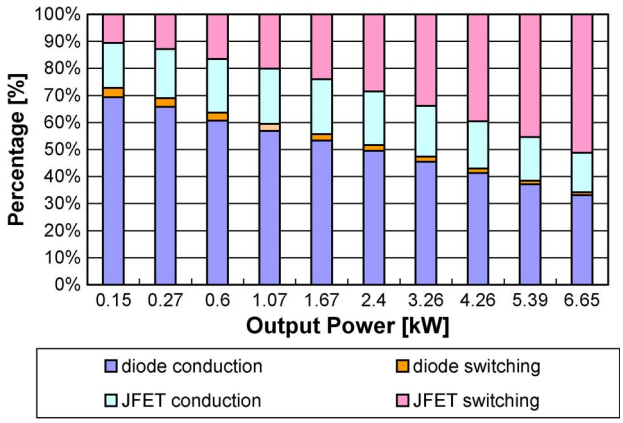

Fig. 12. Percentage of power losses in the SiC inverter at the junction temperature of 100 °C and the switching frequency of 20 kHz.

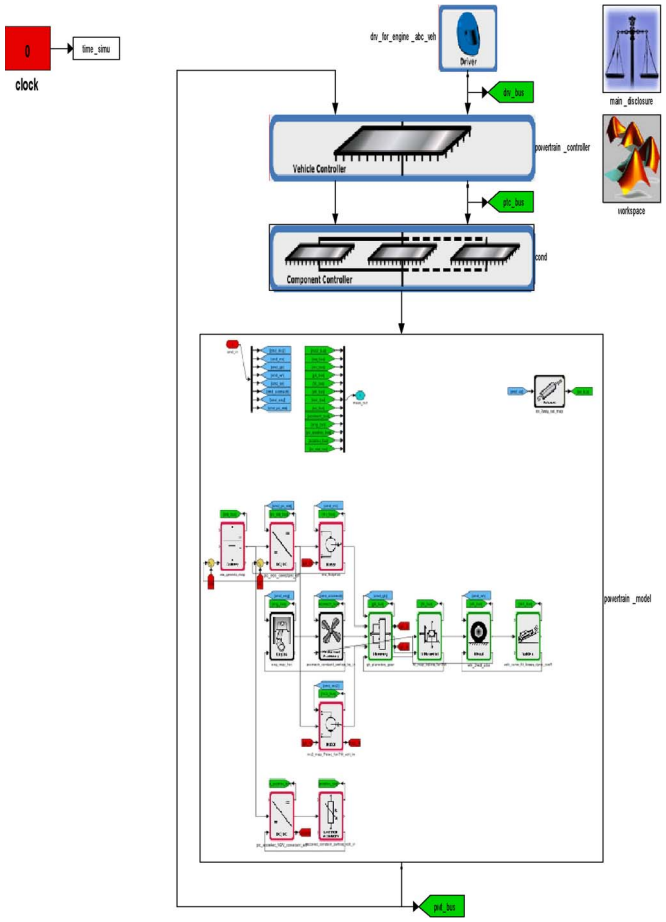

Fig. 13. Simulink model for the HEVs.

IV. HEV

Simulations are run for both a HEV with a SiC inverter and one with a Si inverter for the U.S. Environmental Protection Agency Urban Dynamometer Driving Schedule (UDDS) cycle, which represents city driving conditions of light duty vehicles (see Fig. 14). Assume that the two inverters have the same heat sink size and cooling conditions (ambient temperature is 50 °C), and the switching frequency is 20 kHz. State-of-charge (SOC) correction is performed in order to make the final SOC equal

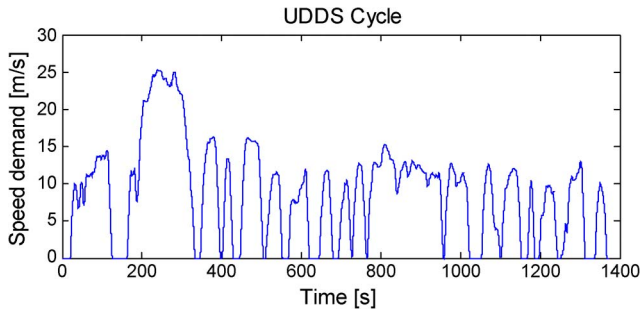

Fig. 14. UDDS cycle.

TABLE II
SUMMARY OF IMPACT OF THE SiC INVERTER ON A HEV (2004 TOYOTA PRIUS)

	Description	Si	SiC	Improve%
Device level	JFETs/IGBTs average junction temperature (°C)	95	58	39.0
	Diodes average junction temperature (°C)	93	58	37.6
	Average inverter power loss (W)	633	116	81.7
	Average inverter efficiency (%)	74.3	89.1	19.9
System level	Fuel economy (liter/100km)	3.94	3.36	14.7
	CO_2 emissions (g/m)	0.09	0.08	11.1
	Energy loss in generator (MJ)	0.31	0.27	12.9
	Energy loss in motor and inverter (MJ)	1.75	1.01	42.3
	Energy loss in mechanical accessory (MJ)	0.15	0.13	13.3
	Energy loss in engine (MJ)	9.9	8.5	14.1
	Total fuel energy use (MJ)	15.1	12.8	13.3
	Percentage braking energy recuperated (%)	65.4	78.7	20.3
	System efficiency (%)	32.9	37.7	14.6
	Mass of fuel needed to travel 515 km (kg)	15.1	12.8	15.2

to the initial SOC. This means that the net energy consumed by the vehicles is fuel energy.

As for the inverter itself, the benefits of the SiC devices are shown in Fig. 15. Due to the lower power losses of the SiC devices, the junction temperatures of the SiC devices are much lower than those of the Si ones [see Fig. 15(a) and (b)]. As a result, the power loss of the SiC inverter is reduced [see Fig. 15(c)], and its efficiency is much improved. The quantified comparisons of SiC and Si inverters are given in Table II.

Furthermore, the benefits of the SiC-based inverter are also seen at the system level. For example, the system efficiency in converting fuel to wheel power is improved from 32.9% to 37.7% (an increase of 14.6%, corresponding to 2.3 MJ for the UDDS drive cycle) due to the energy saving in other powertrain components (such as engine, generator, mechanical accessories, etc.) and the better capability of recuperating braking energy. As a result, the fuel economy is improved from 3.94 to 3.36 L/100 km (fuel consumption decreased by 14.7%). More quantitative results are summarized in Table II.

For the Si-based system, the fuel economy is very close to the manufacturer's data (3.92 L/100 km) even though different Si devices and cooling methods were used in the simulations. For the SiC-based system, the results were based on test results of existing SiC devices but not on a tested complete inverter. While the results may be slightly overestimated, the results are expected to be achieved as improvements are made in these prototype devices.

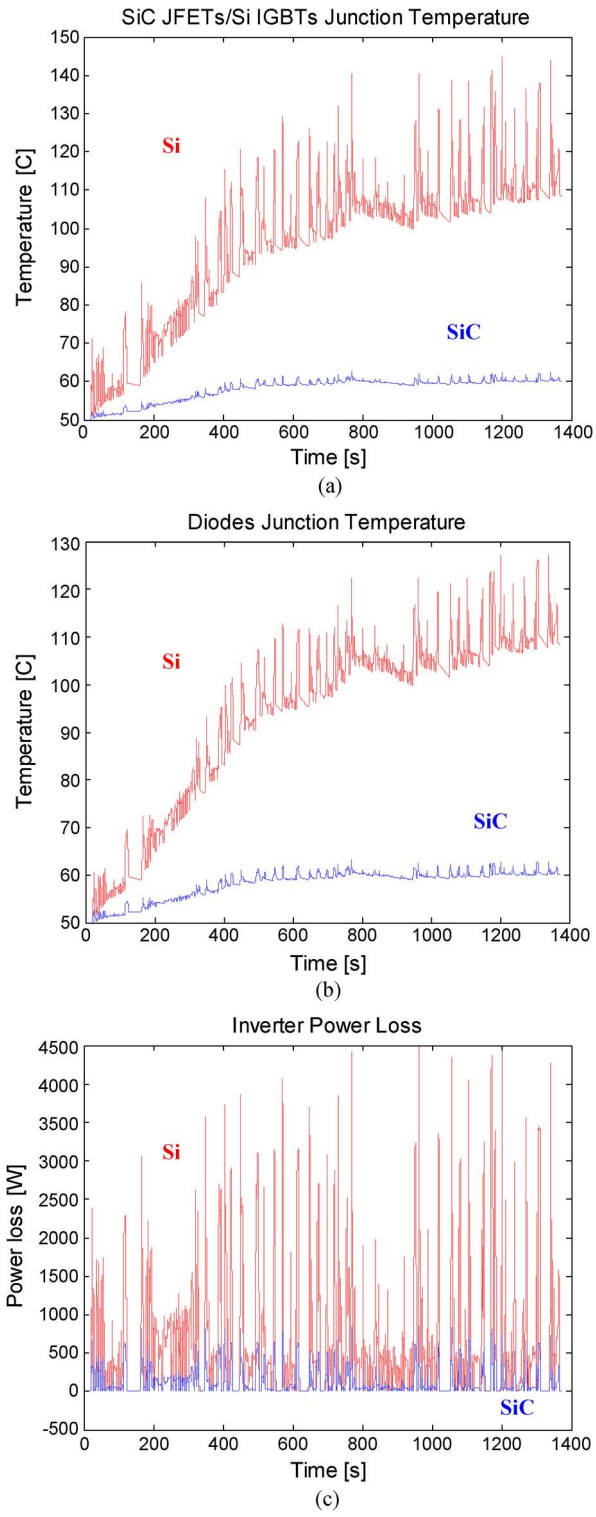

Fig. 15. Comparison of the SiC and Si inverters in the HEV.

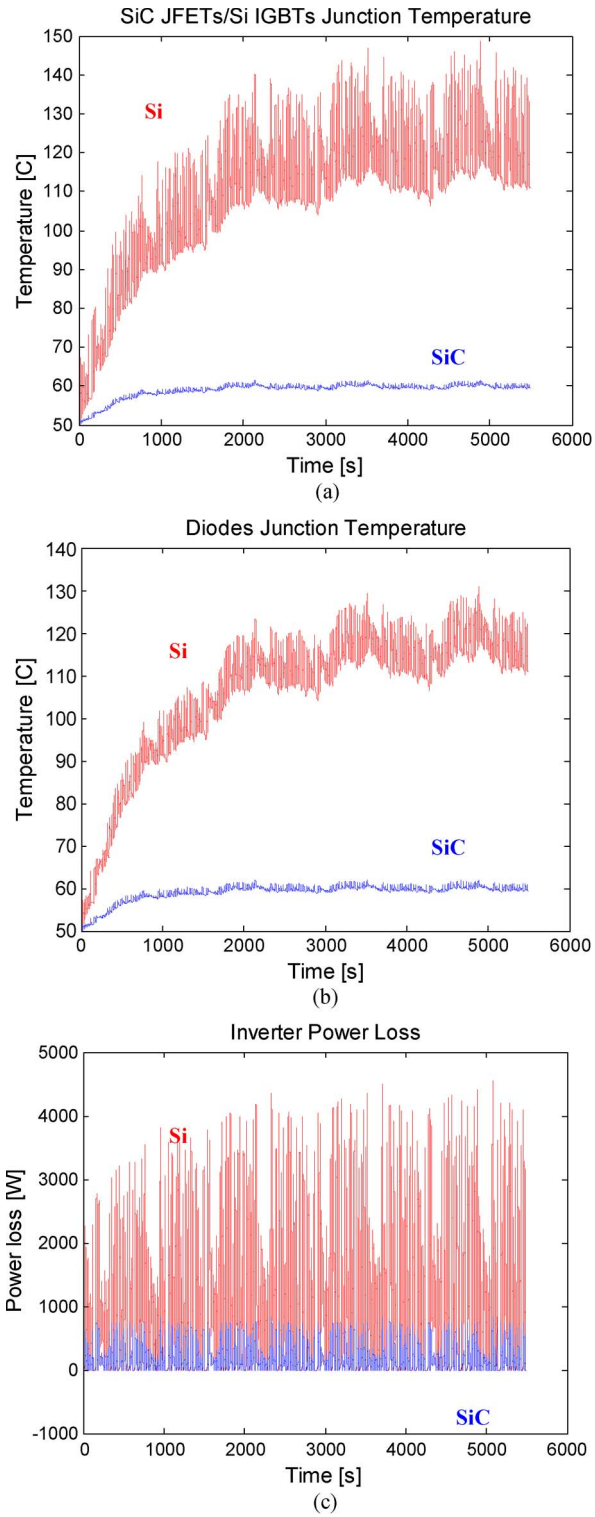

Fig. 16. Comparison of the SiC and Si inverters in the PHEV during AER.

In addition, as shown in Fig. 15(a) and (b), the junction temperatures of the SiC devices are low. Taking into account the high-temperature capability of the SiC devices, the cooling system of the SiC inverter can be downgraded. By simulation, if the size of the heat sink is reduced to half, the efficiency of the inverter will have no substantial change, so the efficiency of the HEV will also not change even with the smaller heat sink.

V. PHEV

A PHEV is designed with all-electric operation capability for several kilometers and functions as a pure electric vehicle during the all-electric range (AER) in urban driving. It has similar components and powertrain architecture with a HEV but has the ability to recharge a larger energy storage system

TABLE III
SUMMARY OF IMPACT OF THE SiC INVERTER ON THE PLUG-IN HEV DURING AER (WITH THE SAME COOLING CONDITION)

	Description	Si	SiC	Improve%
Device level	JFETs/IGBTs average junction temperature (°C)	86	56	34.9
	Diodes average junction temperature (°C)	83	56	32.5
	Average inverter power loss (W)	958	189	80.3
	Average inverter efficiency (%)	72.5	87.1	20.1
System level	Electricity consumption (J/m)	425.1	308.1	27.5
	Energy loss in motor and inverter (MJ)	8.0	2.5	69.1
	Total energy use (MJ)	20.8	15.3	28.6
	Percentage braking energy recuperated (%)	56.7	76.2	34.4
	System efficiency (%)	64.9	78.7	21.3

(such as a battery bank) from off-board electrical power. Thus, PHEVs are more effective in decreasing fuel consumption and reducing air pollution compared to HEVs [30].

The PHEV studied here is designed with a 48-km AER, which is approximately four UDDS cycles. It has the same powertrain architecture and components as the 2004 Toyota Prius HEV, except that the capacity of the battery system is larger. By simulation, the optimized sizes of the battery bank for a plug-in vehicle with the SiC inverter and that with the Si inverter are 5.5 and 7.8 kAh, respectively, compared to 1.1 kAh of the 2004 Toyota Prius HEVs (assume that the initial SOC is 90% and the final SOC is 30%). Thus, for this design, using a SiC-based inverter can reduce the size of the battery bank by 29.5%. Assuming the same heat sink design for both inverters (the size is about twice that of the HEV inverter), simulations are run for both systems for four UDDS cycles. The performance of the two inverters is shown in Fig. 16. Again, due to the lower power losses of the SiC devices, the junction temperatures of the SiC devices are much lower than those of the Si ones [see Fig. 16(a) and (b)]. As a result, the power loss of the SiC inverter is reduced [see Fig. 16(c)], and its efficiency is much improved. The quantified comparison for the SiC and Si inverters is given in Table III.

Furthermore, like the HEV, the benefits of the SiC-based inverter are also seen at the system level. For example, the system efficiency is improved from 64.9% to 78.7% (increased by 21.3%, corresponding to 5.5 MJ for the four driving cycles), and the average electricity consumption during the drive cycle is reduced from 425.1 to 308.1 J/m (decreased by 27.5%). Other quantitative results are summarized in Table III.

Since the junction temperatures of the SiC devices are low, more study is done by reducing the size of the heat sink of the SiC inverter. The junction temperature response is shown in Fig. 17. It is found that the efficiency of the SiC inverter and the system efficiency change very slightly with the smaller heat sink (about 1/6 of the size of the original heat sink). With high-temperature packages, the SiC devices can be used for even higher temperature (at least 200 °C), and further reduced heat sink can be used [31]. Thus, it is feasible to use a small heat sink for the SiC inverter and gain benefits in size and weight.

As a summary, for the PHEVs with optimized design, the application of the SiC inverters can have a small heat sink and battery bank but high system efficiency.

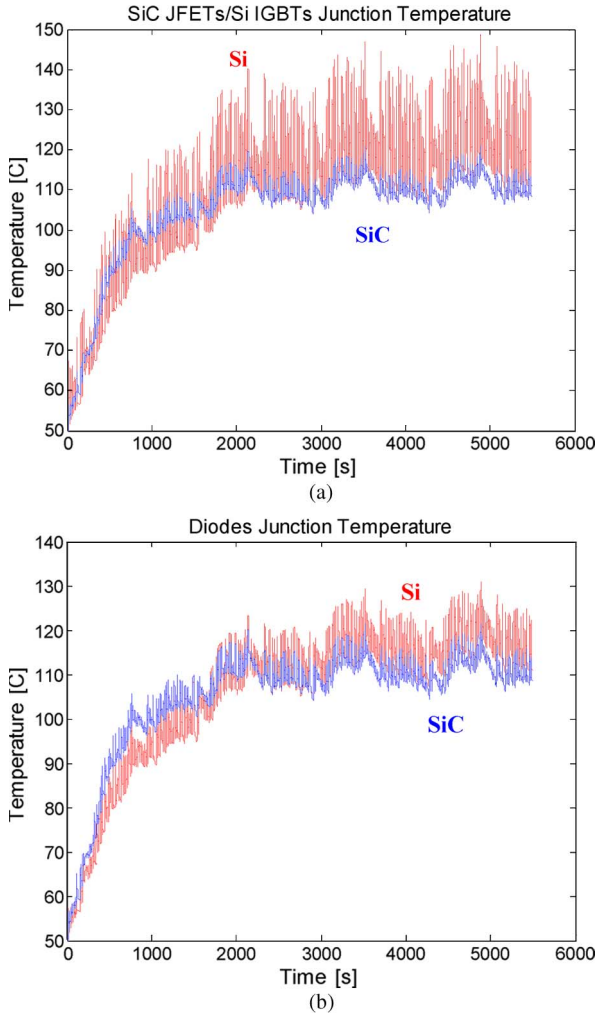

Fig. 17. Junction temperatures of the SiC devices with a smaller heat sink.

To compare with HEVs, the equivalent fuel economy of a PHEV is estimated as follows.

1) Convert electricity economy in AER to equivalent fuel economy. If the energy content of fuel is 32 MJ/L (typical value for 87-octane gasoline), the equivalent fuel economy can be calculated as follows:
PHEV with the SiC inverter

$$\frac{308.1\ \text{J/m}}{32\ \text{MJ/L}} = 0.96\ \text{L}/100\ \text{km} \tag{8}$$

PHEV with the Si inverter

$$\frac{425.1\ \text{J/m}}{32\ \text{MJ/L}} = 1.32\ \text{L}/100\ \text{km}. \tag{9}$$

2) By report [32], for a PHEV with a 48-km AER, the fraction of kilometers potentially displaced by electricity is about 43%. Then, the equivalent fuel economy of a PHEV is the combination of the equivalent fuel economy in AER and the fuel economy in HEV mode since a PHEV works as a HEV outside the AER. The equivalent fuel economies of the two PHEVs are calculated as follows:
PHEV with the SiC inverter

$$0.96 \times 43\% + 3.29 \times 57\% = 2.44\ \text{L}/100\ \text{km} \tag{10}$$

TABLE IV
SYMBOLS

V_D Diode voltage when current is 0	V DC bus voltage
$R_{J,on}$ On-state resistance of JFET	V_0 DC bus voltage for testing
$R_{D,on}$ On-state resistance of diode	I Peak forward current
$P_{Inv,SiC}$ Power loss of SiC inverter	M Modulation index
$P_{J,cond}$ Conduction loss of JFET	ϕ Phase angle of current
$P_{J,sw}$ Switching loss of JFET	f_s Switching frequency
$P_{D,cond}$ Conduction loss of diode	S Snappiness factor of diode
$P_{D,sw}$ Switching loss of diode	$E_{J,sw}$ Switching energy loss of JFET

PHEV with the Si inverter

$$1.32 \times 43\% + 4.24 \times 57\% = 2.98\ \mathrm{L}/100\ \mathrm{km}. \quad (11)$$

In (10) and (11), the second components are the fuel economy of the PHEVs when operating in HEV mode, which are obtained in the same way with the fuel economy of the HEV in Section IV.

Furthermore, the application of the SiC inverter in the PHEV improves the fuel economy by 18.1%, which is larger than that for the conventional HEV (14.7%). It indicates that using a SiC inverter in a PHEV has more impact than in a HEV.

VI. CONCLUSION

The application of the SiC devices in the two HEVs reduces not only the power losses in the motor drive but also those in other components in the vehicle powertrain. As a result, the system efficiency is improved, and the vehicles consume less energy and emit less harmful emissions. It also makes it possible to improve the system compactness with a simplified thermal management system. For the PHEV, the benefits are more distinct. In particular, the size of the battery bank can be reduced for optimum design.

APPENDIX

Table IV shows the symbols of the specific equations for SiC inverters.

REFERENCES

[1] A. Simpson, "Cost-benefit analysis of plug-in hybrid electric vehicle technology," presented at the 22nd Int. Battery, Hybrid Fuel Cell Elect. Vehicle Symp. Exhibit. (EVS-22), Yokohama, Japan, Oct. 23–28, 2006.

[2] M. S. Duvall, "Battery evaluation for plug-in hybrid electric vehicles," in *Proc. IEEE Vehicle Power Propulson Conf.*, Chicago, IL, Sep. 7–9, 2005, pp. 338–343.

[3] C. W. Ayers, J. S. Hsu, L. D. Marlino, C. W. Miller, G. W. Ott, Jr., and C. B. Oland, "Evaluation of 2004 Toyota Prius hybrid electric drive system interim report," Oak Ridge Nat. Lab., UT-Battelle, Oak Ridge, TN, ORNL/TM-2004/247, Nov. 2004.

[4] F. An, A. Vyas, J. Anderson, and D. Santini, "Evaluating commercial and prototype HEVs," presented at the SAE World Congr., Detroit, MI, Mar., 2001.

[5] S. Inman, M. El-Gindy, and D. C. Haworth, "Hybrid electric vehicles technology and simulation: Literature review," *Int. J. Heavy Vehicle Syst.*, vol. 10, no. 3, pp. 167–187, Jul. 2003.

[6] N. Nozawa, T. Maekawa, S. Nozawa, and K. Asakura, "Development of power control unit for compact-class vehicle," presented at the SAE World Congr. Exhibit., Detroit, MI, Apr., 2009, SAE 2009-01-1310.

[7] R. Kelley, M. S. Mazzola, and V. Bondarenko, "A scalable SiC device for dc/dc converters in future hybrid electric vehicles," in *Proc. IEEE Appl. Power Electron. Conf. Expo.*, Dallas, TX, Mar. 19–23, 2006, pp. 460–463.

[8] B. Wrzecionko, J. Biela, and J. W. Kolar, "SiC power semiconductors in HEVs: Influence of junction temperature on power density, chip utilization and efficiency," in *Proc. 35th Annu. Conf. IEEE Ind. Electron.*, Porto, Portugal, Nov. 3–5, 2009, pp. 3834–3841.

[9] A. T. Bryant, G. J. Roberts, A. Walker, and P. A. Mawby, "Fast inverter loss simulation and silicon carbide device evaluation for hybrid electric vehicle drives," in *Proc. Power Convers. Conf.*, Nagoya, Japan, Apr. 2–5, 2007, pp. 1017–1024.

[10] A. Antonopoulos, H. Bangtsson, M. Alakula, and S. Manias, "Introducing a silicon carbide inverter for hybrid electric vehicles," in *Proc. Power Electron. Spec. Conf.*, Rhodes, Greece, Jun. 15–19, 2008, pp. 1321–1325.

[11] Powertrain System Analysis Toolkit (PSAT) Advanced Features, Argonne Nat. Lab. Argonne, IL.

[12] H. Zhang, L. M. Tolbert, and B. Ozpineci, "Impact of SiC devices on hybrid electric and plug-in hybrid electric vehicles," in *Conf. Rec. IEEE IAS Annu. Meeting*, Edmonton, AB, Canada, Oct. 5–9, 2008, pp. 1–5.

[13] Silicon Carbide Diode (1200 V/10 A) Datasheet. [Online]. Available: http://www.cree.Com/products/pdf/C2D10120.pdf

[14] H. Zhang, L. M. Tolbert, B. Ozpineci, and M. Chinthavali, "Power losses and thermal modeling of 4H-SiC VJFET inverter," in *Conf. Rec. IEEE IAS Annu. Meeting*, Hong Kong, China, Oct. 2–6, 2005, pp. 2630–2634.

[15] H. Zhang, L. M. Tolbert, and B. Ozpineci, "System modeling and characterization of SiC Schottky power diodes," in *Proc. IEEE Workshop Comput. Power Electron.*, Troy, NY, Jul. 16–19, 2006, pp. 199–204.

[16] P. Friedrichs, "Silicon carbide power devices—Status and upcoming challenges," in *Proc. Eur. Conf. Power Electron. Appl.*, Aalborg, Denmark, Sep. 2–5, 2007, pp. 1–11.

[17] R. J. Callanan, A. Agarwal, A. Burk, M. Das, B. Hull, F. Husna, A. Powell, J. Richmond, S. Ryu, and Q. Zhang, "Recent progress in SiC DMOSFETs and JBS diodes at Cree," in *Proc. Annu. Conf. IEEE Ind. Electron.*, Orlando, FL, Nov. 10–13, 2008, pp. 2885–2890.

[18] Y. Sugawara, D. Takayama, K. Asano, S. Ryu, A. Miyauchi, S. Ogata, and T. Hayashi, "4H-SiC high power SIJFET module," in *Proc. IEEE 15th Int. Symp. Power Semicond. Devices ICs*, Apr. 14–17, 2003, pp. 127–130.

[19] T. E. Salem, D. P. Urciuoli, R. Green, and G. K. Ovrebo, "High-temperature high-power operation of a 100 A SiC DMOSFET module," in *Proc. IEEE Appl. Power Electron. Conf. Expo.*, Washington, DC, Feb. 15–19, 2009, pp. 653–657.

[20] J. M. Ortiz-Rodriguez, M. Hernandez-Mora, T. H. Duong, S. G. Leslie, and A. R. Hefner, "Thermal network component models for 10 kV SiC power module packages," in *Proc. IEEE Power Electron. Spec. Conf.*, Rhodes, Greece, Jun. 15–19, 2008, pp. 4770–4775.

[21] Cree and Powerex Develop New SiC Power Switches for Next-Generation Military Systems, Durham, NC, Feb. 17, 2009. Press release. [Online]. Available: www.cree.com/press/press_detail.asp?i=1234879464387

[22] T. Nezu, Rohm Exhibits New SiC Power Module, Oct. 16, 2009. Techon Newsletter. [Online]. Available: http://techon.nikkeibp.co.jp/english/NEWS_EN/20091016/176491/

[23] J. Richmond, S. Leslie, B. Hull, M. Das, A. Agarwal, and J. Palmour, "Roadmap for megawatt class power switch modules utilizing large area silicon carbide MOSFETs and JBS diodes," in *Proc. IEEE Energy Convers. Congr. Expo.*, San Jose, CA, Sep. 20–24, 2009, pp. 106–111.

[24] B. Opzineci, "System impact of silicon carbide power electronics on hybrid electric vehicle applications," Ph.D. dissertation, Univ. Tennessee, 2002.

[25] F. Blaabjerg, U. Jaeger, and S. Munk-Nielsen, "Power losses in PWM-VSI inverter using NPT or PT IGBT devices," *IEEE Trans. Power Electron.*, vol. 10, no. 3, pp. 358–367, May 1995.

[26] T. Hopkins, C. Cognetti, and R. Tiziani, "Designing with thermal impedance," in *Proc. 4th Annu. IEEE Semiconductor Thermal Temp. Meas. Symp.*, San Diego, CA, Feb. 10–12, 1988, pp. 55–61.

[27] H. Zhang, L. M. Tolbert, B. Ozpineci, and M. Chinthavali, "A SiC-based converter as a utility interface for a battery system," in *Conf. Rec. IEEE IAS Annu. Meeting*, Tampa, FL, Oct. 8–12, 2006, pp. 346–350.

[28] V. Blasko, R. Lukaszewski, and R. Sladky, "On line thermal model and thermal management strategy of a three phase voltage source inverter," in *Conf. Rec. IEEE IAS Annu. Meeting*, Phoenix, AZ, Oct. 3–7, 1999, pp. 1423–1431.

[29] H. Zhang, L. M. Tolbert, J. H. Han, M. S. Chinthaval, and F. Barlow, "18 kW three phase inverter system using hermetically sealed

SiC phase-leg power modules," in *Proc. IEEE Appl. Power Electron. Conf. Expo.*, Palm Springs, CA, Feb. 21–25, 2010, pp. 1108–1112.

[30] A. Francisco and A. A. Frank, *Drive System Analysis and Optimization for Plug-in Hybrid Electric Vehicles*. Davis, CA: Univ. California-Davis, 2001.

[31] H. Tokuda, Y. Tanaka, H. Nakagawa, M. Aoyagi, K. Fukuda, H. Ohashi, T. Tsuno, T. Hoshino, Y. Namikawa, and H. Hayashi, "Investigation of a SiC module with a high operating temperature for power applications," in *Proc. Electron. Packag. Technol. Conf.*, Singapore, Dec. 10–12, 2007, pp. 931–936.

[32] P. Denholm and W. Short, An evaluation of utility system impacts and benefits of optimally dispatched plug-in hybrid electric vehicles, Tech. Rep. NREL/TP-620-40 293. [Online]. Available: http://www.nrel.gov/docs/fy07osti/40293.pdf

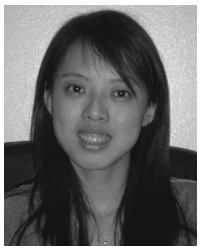

Hui Zhang (S'03–M'07) received the B.S. and M.S. degrees in electrical engineering from Zhejiang University, Hangzhou, China, in 2000 and 2003, respectively, and the Ph.D. degree in electrical engineering from The University of Tennessee, Knoxville, in 2007.

In 2005, she was a Student Member at the Power Electronics and Electric Machinery Research Center, Oak Ridge National Laboratory, Knoxville. From 2007 to 2009, she was a Postdoctoral Research Associate at The University of Tennessee and Oak Ridge National Laboratory. She is currently an Assistant Professor in the Electrical Engineering Department, Tuskegee University, Tuskegee, AL.

Dr. Zhang is a member of the IEEE Power Electronics, IEEE Industry Applications, and IEEE Industrial Electronics Societies. She has served as a Reviewer for several IEEE TRANSACTIONS and as Session Chair for IEEE conferences.

Leon M. Tolbert (S'88–M'91–SM'98) received the B.S., M.S., and Ph.D. degrees in electrical engineering from the Georgia Institute of Technology, Atlanta, in 1989, 1991, and 1999, respectively.

In 1991, he joined the Engineering Division, Oak Ridge National Laboratory, Oak Ridge, TN. In 1999, he became an Assistant Professor in the Department of Electrical and Computer Engineering, The University of Tennessee, Knoxville. He is currently the Min Kao Professor in the Department of Electrical Engineering and Computer Science, The University of Tennessee. He is also a Research Engineer at the Power Electronics and Electric Power Systems Research Center, Oak Ridge National Laboratory, Knoxville.

Dr. Tolbert is a Registered Professional Engineer in the State of Tennessee. From 2003 to 2006, he was the Chairman of the Education Activities Committee of the IEEE Power Electronics Society and an Associate Editor for the IEEE POWER ELECTRONICS LETTERS. He has been an Associate Editor of the IEEE TRANSACTIONS ON POWER ELECTRONICS since 2007. He was elected to serve as a Member-at-Large of the IEEE Power Electronics Society Advisory Committee for 2010–2012. He was a recipient of a National Science Foundation CAREER Award in 2001, the 2001 IEEE Industry Applications Society Outstanding Young Member Award, and three prize paper awards from the IEEE Industry Applications Society and IEEE Power Electronics Society.

Burak Ozpineci (S'92–M'02–SM'05) received the B.S. degree in electrical engineering from the Middle East Technical University, Ankara, Turkey, in 1994, and the M.S. and Ph.D. degrees in electrical engineering from The University of Tennessee, Knoxville, in 1998 and 2002, respectively.

He is currently with the Power Electronics and Electric Power Systems Research Center, Oak Ridge National Laboratory (ORNL), Knoxville, where he joined the Postmasters Program in 2001, became a Full-Time Research and Development Staff Member in 2002, and has been the Group Leader of the Power and Energy Systems Group since 2008. He is also an Adjunct Professor at the University of Arkansas, Fayetteville, and The University of Tennessee, Knoxville. He is conducting research on the system-level impact of SiC power devices, multilevel inverters, power converters for distributed energy resources and hybrid electric vehicles, and intelligent control applications for power converters.

Dr. Ozpineci was the Chair of the IEEE Power Electronics Society Rectifiers and Inverters Technical Committee and the TRANSACTIONS Review Chairman of the IEEE Industry Applications Society Industrial Power Converter Committee. He was the recipient of the 2006 IEEE Industry Applications Society Outstanding Young Member Award, the 2001 IEEE International Conference on Systems, Man, and Cybernetics Best Student Paper Award, and the 2005 UT-Battelle (ORNL) Early Career Award for Engineering Accomplishment.